

Cylindrical scaling for dynamical cooling models of the Earth

Peter van Keken*

Department of Geological Sciences, 425 E University, 2534 CC Little Building, University of Michigan, Ann Arbor, MI 48109-1063, USA

Received 6 October 2000; accepted 7 March 2001

Abstract

A detailed comparison is presented between axisymmetric spherical shell and cylindrical geometry for use in mantle convection modeling. If a rescaling of the mantle and core radii is adopted, such that the curvature of the cylindrical model approximates that of the spherical Earth, the heat and mass transport properties turn out to be very similar. Without the scaling, the volume of the lower mantle and the surface area of the core are overestimated, which leads to incorrect estimates of heat production and heat flow. This is particularly important for thermal evolution models. An explicit comparison with parameterized convection calculations shows that the scaling used here provides a good approach to dynamical model calculations. © 2001 Elsevier Science B.V. All rights reserved.

Keywords: Mantle convection; Modeling; Numerical methods; Finite elements

1. Introduction

Thermal cooling models are essential for our understanding of the thermal and chemical evolution of the Earth. Previous studies have used parameterized convection simulations (e.g. Spohn and Schubert, 1982; Christensen, 1985; McNamara and Van Keken, 2000) that include the appropriate effects of radiogenic heating and secular cooling in a spherical geometry. The main drawback is the necessary parameterization of the relationship between heat loss and dynamical parameters, which makes it difficult to assess the influence of many aspects that are considered important for the dynamics of the Earth. These include: (1) spatially variable properties such as rheology, expansivity, and conductivity; (2) compressible effects such as viscous heating and adiabatic heating and cooling; (3) the influence of the mantle transition zone; (4) the

effects of continents and changes in tectonic style. Due to improved computer and software availability, full dynamical modeling by solution of the governing mass and heat transfer equations has become an important alternative to parameterized convection.

We have made significant progress in the last decade with 3D spherical models (e.g. Bercovici et al., 1989; Tackley et al., 1993; Zhang and Yuen, 1996; Bunge et al., 1996), but the use of this geometry for calculations at realistic convective vigor are still very expensive, and currently prohibitively so for evolution models that by necessity must span a significant portion of the age of the Earth. This explains the popularity and widespread use of simplifying geometries which include those of the axisymmetric spherical shell, cylinder, and 2D or 3D Cartesian box (Fig. 1). In most cases, the approximation involves a straightening of the curved state of the Earth, either in only one dimension, which leads to a cylinder, or in both to yield a Cartesian geometry. These simplifications come at a cost. The axisymmetric spherical

* Tel.: +1-734-764-1497; fax: +1-734-763-4690.
E-mail address: keken@umich.edu (P. van Keken).

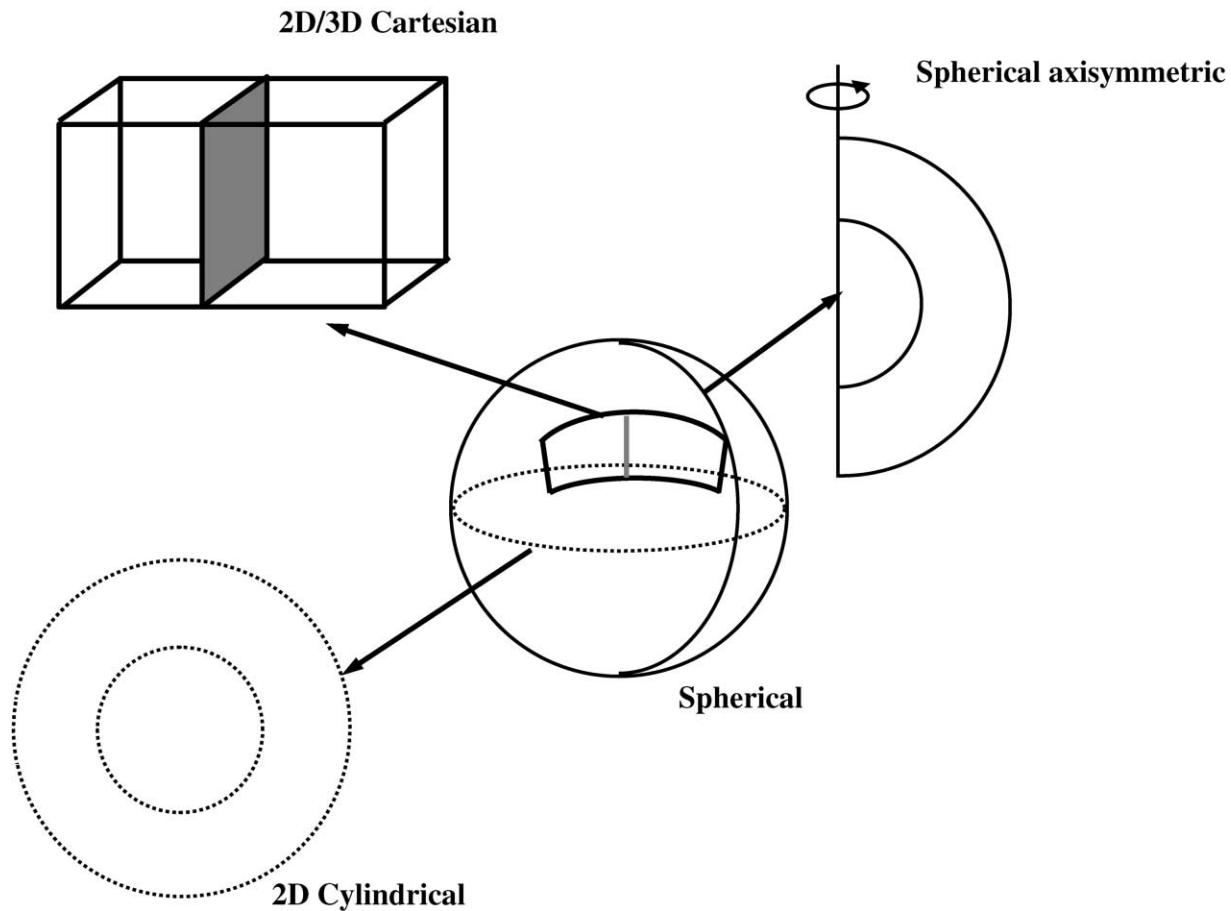


Fig. 1. Comparison of common approximations to the 3D spherical geometry of the Earth.

geometry has found some use in convection modeling (Solheim and Peltier, 1994; Van Keken and Yuen, 1995), as it best approximates the curvature of the spherical Earth, but due to the rotational symmetry a rather awkward asymmetry between polar regions and equatorial plane exists. This causes the dynamics to be governed by the volumetrically more important equatorial region. In addition, the poles form artificial boundaries where up- or down-welling plumes tend to get trapped. Cartesian models arise from the complete straightening of the curved geometry and are very popular (e.g. Tackley, 2000) due to the simpler form of the equations, ease of discretization and widespread availability of programs or libraries for the solution of partial differential equations in this geometry. However, the lack of curvature has some

important consequences. For example, Cartesian models overestimate the volume of deep layers as well as the surface area of the core–mantle boundary. This makes this geometry ill-suited for accurate evaluation of thermal evolution models. The cylinder geometry is based on an intermediate approach, where the spherical model is straightened in only one direction. The assumption of cylinder symmetry reduces the geometry to 2D with associated lower computational cost. The advantage of this approach is that similar to the spherical case the geometry is a simply connected region without artificial boundaries.

In this paper, we will explore the use of a particular scaling of the cylindrical geometry which arrives from making the ratio of surface area of core and mantle the same as in the spherical geometry, which

provides a closer approximation to the curvature of the Earth. A simple boundary layer analysis for bottom-heated convection with constant properties showed that this leads to an improved approximation to the heat-transport characteristics of spherical models (Vangelov and Jarvis, 1994). Here, we will provide further evidence that the heat and mass transfer of cylindrical models is very similar to that of spherical models using a number of simple benchmarks that incorporate internal heating and compressible convection. This similarity opens up the possibility of using 2D cylindrical models for studying the thermal cooling of the Earth, and provides therefore an ideal alternative to offset the high cost of 3D spherical models, while avoiding problems with the interpretation of results obtained on Cartesian grids.

2. Model formulation and numerical approach

In this paper, we are concerned with the solution of the equations governing convection in the Earth's mantle, assuming that the mantle can be described as an anelastic and weakly compressible fluid at infinite Prandtl number. Assuming the extended Boussinesq approach, we can write the equations of motion as

$$-\nabla P + \nabla \cdot (\eta \dot{\epsilon}) = Ra \alpha \rho T \hat{\mathbf{g}} \quad (1)$$

and the mass conservation equation as

$$\nabla \cdot \mathbf{u} = 0 \quad (2)$$

The heat equation incorporates terms that describe viscous heating and adiabatic cooling and heating, and can be written as

$$\frac{\partial T}{\partial t} + (\mathbf{u} \cdot \nabla)T + \alpha Di w T = \nabla \cdot (\kappa \nabla T) + Q + \frac{Di}{Ra} \sigma_{ij} \frac{\partial u_i}{\partial x_j} - \alpha Di w T_0 \quad (3)$$

(e.g. Jarvis and McKenzie, 1980; Ita and King, 1994). Note that the extended Boussinesq approach includes the assumption that the density ρ is constant in the equations of conservation of mass (2) and heat (3). The equations above are non-dimensional. The symbols representing physical quantities and their non-dimensionalization are explained in Table 1.

Table 1
Dimensionless quantities

| Symbol | Quantity | Non-dimensionalization |
|--------------------|--|--------------------------------------|
| P | Dynamic pressure | $h^2/\eta_0\kappa_0$ |
| η | Dynamic viscosity | η_0 |
| $\dot{\epsilon}$ | Deviatoric strain rate tensor | h^2/κ_0 |
| α | Thermal expansivity | α_0 |
| ρ | Density | ρ_0 |
| T | Temperature | ΔT_0 |
| $\hat{\mathbf{g}}$ | Unit vector in the direction of gravity | g |
| \mathbf{u} | Velocity vector with components u_i | κ_0/h |
| w | Upward velocity component | κ_0/h |
| σ_{ij} | Components of the deviatoric stress tensor | $h^2/\eta_0\kappa_0$ |
| t | Time | h^2/κ_0 |
| k | Thermal conductivity | k_0 |
| κ | Thermal diffusivity ($k/\rho c_p$) | $\kappa_0 = k_0/\rho_0 c_p$ |
| Q | Volumetric radiogenic heating | $h^2/c_p \kappa_0 \Delta T_0 \rho_0$ |
| T_0 | Surface temperature | ΔT_0 |

The Rayleigh number, Ra , and dissipation number, Di , are given by

$$Ra = \frac{\rho_0 g \alpha_0 \Delta T h^3}{\eta_0 \kappa_0} \quad (4)$$

and

$$Di = \frac{\alpha_0 g h}{c_p} \quad (5)$$

The quantities on the right-hand sides are dimensional and are explained in Table 2.

We will compare the thermal and mass transport characteristics of the cylindrical and spherical geometry. In an effort to reduce the effects of differences in convection planform (e.g. aspect ratio, orientation of rolls), we use the domains shown in Fig. 2, assuming

Table 2
Dimensional constants

| Symbol | Quantity | Value |
|--------------|---|--------------------|
| ρ_0 | Reference mantle density (kg/m ³) | 4500 |
| g | Gravitational acceleration (m/s ²) | 9.8 |
| α_0 | Surface thermal expansivity (K ⁻¹) | 3×10^{-5} |
| κ_0 | Average thermal diffusivity (m ² /s) | 10^{-6} |
| ΔT_0 | Temperature contrast across mantle (K) | 3000 |
| h | Depth of the mantle (km) | 2885 |
| η_0 | Reference mantle viscosity (Pa s) | 10^{22} |
| c_p | Mantle specific heat (J/K kg) | 1250 |

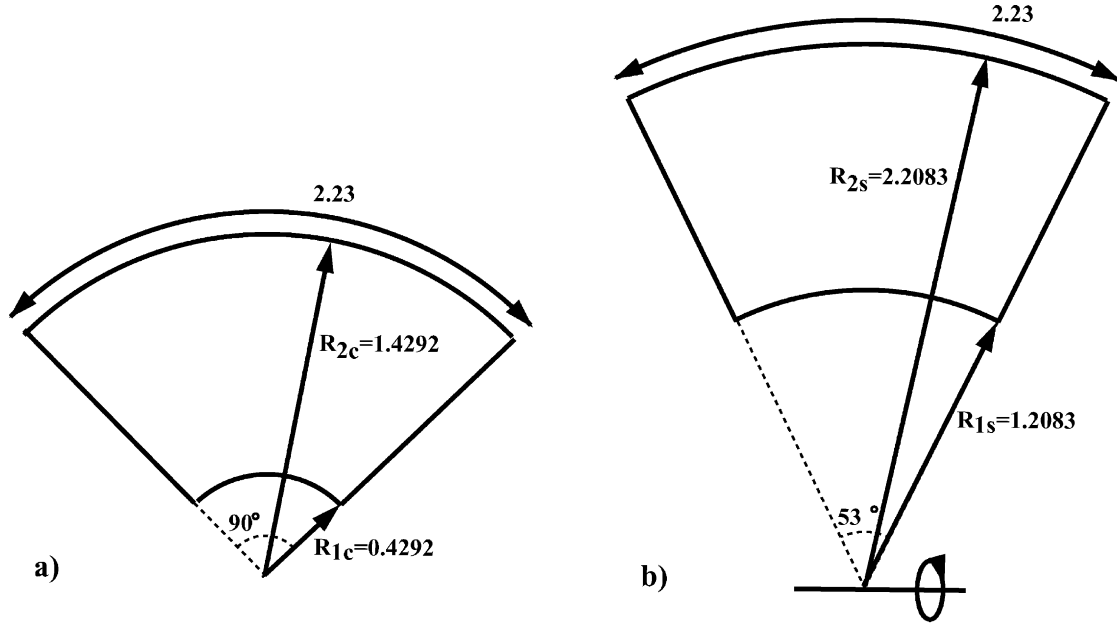


Fig. 2. Comparison of the axisymmetric spherical and cylindrical geometries used in this study. The radii of the core and mantle in the cylindrical model (a) have been rescaled to conserve the appropriate ratio of mantle and core surfaces.

axisymmetry for the spherical model. The non-dimensional radii for the spherical model are based on an average Earth radius of 6371 km and average core–mantle boundary radius of 3486 km. Demanding the non-dimensional depth of the mantle to be 1 leads to non-dimensional inner radius $R_{1s} = 1.2083$, and outer radius $R_{1s} = 2.2083$. The inner and outer radii of the cylinder geometry are chosen such that the ratio of the surface area of core and mantle is the same in the two geometries, that is

$$\frac{R_{2s}^2}{R_{1s}^2} = \frac{R_{2c}}{R_{1c}} = 3.33 \quad (6)$$

from which it follows $R_{1c} = 0.4292$ and $R_{1c} = 1.4292$. For the cylindrical model, we use a 90° segment, such that the length of the upper arc is $\pi R_{2c}/2 = 2.23$. To maintain a similar aspect ratio (upper arc length) in the spherical model, we use a segment of 53° , centered around the equator (Fig. 2).

To mimic the full effects of compressibility, we assume variable thermal conductivity k and expansivity α , using the relations

$$\alpha(z) = \rho(z)^{-2} \quad (7)$$

and

$$k(z) = \left(\frac{\rho(z)}{\langle \rho \rangle} \right)^3 \quad (8)$$

where the density is given by

$$\rho(z) = e^{Di z/\gamma} \quad (9)$$

and z is the non-dimensional depth, normalized by the depth of the mantle and γ is the Grüneisen parameter. This formulation is similar to that employed in Leitch et al. (1991). We will use $Di = 0.5$ and $\gamma = 1$. The average density $\langle \rho \rangle$ depends on the geometry. For example,

$$\langle \rho \rangle = \frac{\iint \rho r^2 dr d\theta}{\iint r^2 dr d\theta} \quad (10)$$

for axisymmetric spherical (where θ is latitude) and

$$\langle \rho \rangle = \frac{\int \rho r dr}{\int r dr} \quad (11)$$

for cylindrical. As a consequence, the depth range of k and α are different with resulting differences in the heat transport. However, the rescaling of the cylindrical model strongly minimizes the differences. In this case, the average density is 1.236 (compared to 1.239 for spherical), the surface and CMB values of conductivity are 0.525 and 2.353 (compared to 0.529 and 2.371), and the CMB value for expansivity is 0.3679 (compared to 0.3679). The conductive heat flow is a function of both the conductivity and the geometry, which is illustrated by the larger, but acceptable, differences in the values of the conductive heat flow out of top and bottom, 0.679 and 2.273 (compared to 0.646 and 2.165, respectively).

The Eqs. (1)–(3) are solved using a finite element approach based on the general tool box Sepran (Cuvelier et al., 1986; <http://dutita0.twi.tudelft.nl/sepran/sepran.html>) which has been used extensively for the modeling of mantle convection in Cartesian (Van den Berg et al., 1993), axisymmetric spherical (Van Keken and Yuen, 1995), and cylindrical geometries (Van Keken and Ballentine, 1999). The Stokes Eq. (1) and incompressibility constraint (2) are solved using a penalty function approach. The heat equation is solved using a Petrov–Galerkin discretization. Stationary solutions are computed by explicitly setting the time derivative in Eq. (3) to 0. The time-dependent equations are solved using a second-order predictor–corrector method. See Van den Berg et al. (1993) for more details. The numerical implementation has been extensively tested against standard mantle convection benchmarks (Blankenbach et al., 1989; Busse et al., 1993; Van Keken et al., 1997) as well as published results by other workers (e.g. Mouchetel and Yuen, 1988; Jarvis, 1994), which is important in the case of cylindrical and axisymmetric spherical geometry for which no published benchmarks exist.

3. Comparison of heat and mass transport characteristics

In this section, we will demonstrate the strong similarities of the heat and mass transport of the spherical and rescaled cylindrical geometries. We will first explore steady state bottom and internally heated convection models, followed by a time-dependent

benchmark. In all cases, we will use $Di = 0.5$ and α and k are depth-dependent following Eqs. (7) and (8). We will first make the additional simplifying assumptions that $\rho = 1$ in the right-hand side of Eq. (1) and the volumetric heating rate Q a constant. This is a deviation from the extended Boussinesq approximation that includes these as depth-dependent quantities. The further approximation has an influence on the pattern of the flow because of the redistribution of radiogenic heating and buoyancy forces. Particularly, the change in volumetric heating rate may have a strong influence due to its dynamic feedback through temperature-dependent viscosity. However, it is important to note at this point that it is not our intention to discuss the impact of the varying degrees to which we can approximate the full compressible equations. This has been done quite well elsewhere (e.g. Ita and King, 1994). Our main focus here is to show the properties of the rescaled cylindrical geometry by comparing results side-by-side to the axisymmetric case for the same given set of approximations. We will do the comparison for a wide variety of assumptions that include incompressible Boussinesq with constant α and k , extended Boussinesq with depth-dependent α and k , and constant and temperature-dependent viscosity. After the first set of comparisons, we will also include the depth dependence of ρ in Eq. (1) and Q in Eq. (3).

Table 3 compares the heat-transport characteristics for steady state solutions of the type shown in Fig. 3 for the two geometries. The bottom boundary is at constant temperature $T = 1$, the top boundary condition is at $T = 0$, and the side boundaries are reflective. Free-slip boundary conditions are imposed at all boundaries. The viscosity of the fluid is held constant at $\eta = 1$. The comparison is limited to low Ra , because at increasing convecting vigor it is generally not possible to arrive at a steady state for these models. The non-dimensional surface heat flow is relatively low, due to the low Ra in combination with the low surface conductivity. To compare, the present day mantle heat flow of the Earth is on average 74 mW/m^2 which scales in this case to a non-dimensional heat flow of 12. The mantle heat flow value is based on the global surface heat flow average (44 TW; Pollack et al., 1993) minus an estimated contribution from the continental crust (6 TW; e.g. Van Schmus, 1995).

Note, the good agreement of the general transport characteristics. The surface and core heat flow values,

Table 3
Comparison of bottom-heated convection

| Geometry | Ra | q_t^a | q_c^b | v_{rms}^c | v_{max}^d | $\langle v \rangle^e$ | $\langle \Phi \rangle^f$ |
|-------------|-----------------|---------|---------|-------------|-------------|-----------------------|--------------------------|
| Cylindrical | 5×10^4 | 3.11 | 10.35 | 77.2 | 121 | 99.5 | 1.19 |
| | 10^5 | 3.72 | 12.42 | 114.5 | 178 | 148 | 1.51 |
| | 2×10^5 | 4.48 | 14.96 | 170.5 | 268 | 222 | 1.88 |
| Spherical | 5×10^4 | 3.08 | 10.31 | 79.7 | 110 | 91 | 1.27 |
| | 10^5 | 3.68 | 12.28 | 117.1 | 163 | 135 | 1.57 |
| | 2×10^5 | 4.40 | 14.64 | 171.9 | 245 | 197 | 1.94 |

^a Mantle heat flow.

^b Core heat flow.

^c rms velocity.

^d Maximum surface velocity.

^e Average surface velocity.

^f Average viscous dissipation.

as well as the rms velocity agree to within a few percent. The difference is somewhat larger for the surface velocity, which is overpredicted by up to 10% in the cylindrical model.

In the case of internal heating, we need to take into consideration that the non-dimensional surface-to-volume ratio (S/V) of the two approaches

is slightly different. For the axisymmetric spherical case $S/V = 1.625$, which is 5.6% higher than that of the cylindrical model ($S/V = 1.538$). If we would use the same values for radiogenic heat production, we would find a higher surface heat flow in the cylindrical case. Although this difference is small, it is sufficiently small to attempt a correction. The simplest approach is to reduce the radiogenic heat production proportionally in the cylindrical case, which is what we have done in the internally heated cases below.

Fig. 4 and Table 4 show a comparison of internally heated cases with insulated lower boundary. Internal heating rates are $Q = 10$ for cylindrical and $Q = 10.56$ for spherical. Again, the derived quantities agree to within a few percent.

A more strenuous test of the applicability of this cylindrical scaling is by using temperature-dependent rheology. For the results displayed in Fig. 5 and Table 5, we have used a temperature-dependent rheology of the form

$$\eta(T) = \exp\left(\frac{E}{T + T_0} - \frac{E}{1 + T_0}\right) \quad (12)$$

with $E = 1.66$ and $T_0 = 0.2$. This gives a variation of about three orders of magnitude of viscosity. Although, we might have predicted that the added nonlinear dependence of viscosity on temperature would lead to less representative results, the surface and bottom heat flow as well as the rms velocity agree to within 4% between the two geometries.

A further test of the scaling involves time dependence. Here, we have used a model similar to the

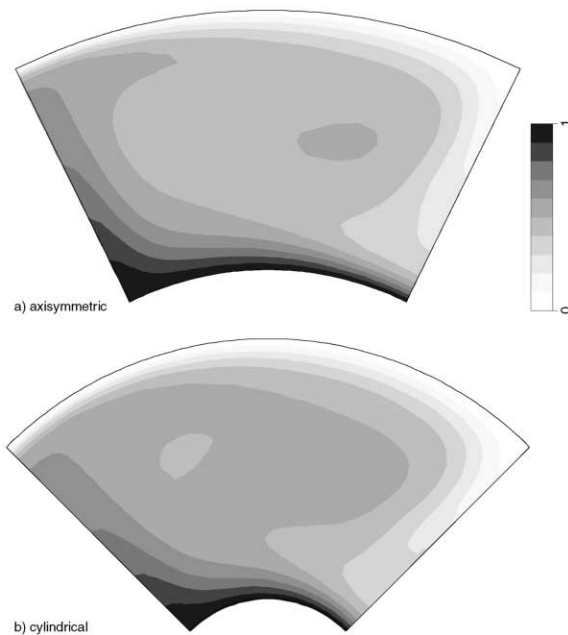


Fig. 3. Comparison of temperature in steady state bottom-heated convection in axisymmetric (a) and cylindrical geometry (b); $Ra = 5 \times 10^4$.

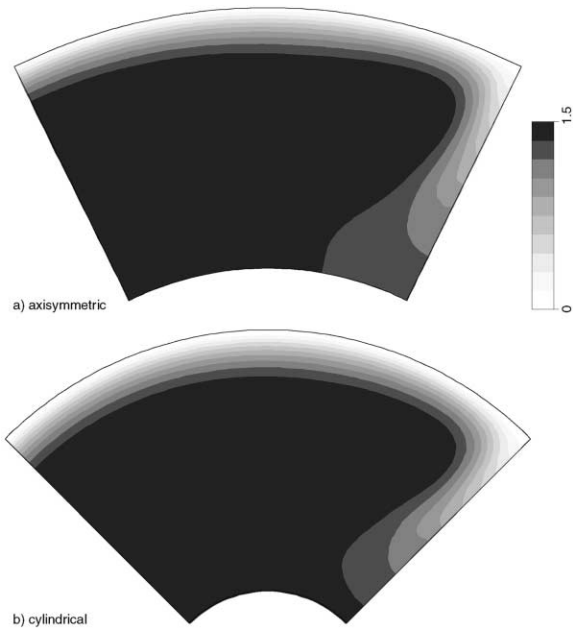


Fig. 4. Comparison of temperature in steady state internally heated convection in axisymmetric (a) and cylindrical geometry (b); $Ra = 2 \times 10^4$, $Q = 10$ (cylindrical), $Q = 10.6$ (axisymmetric).

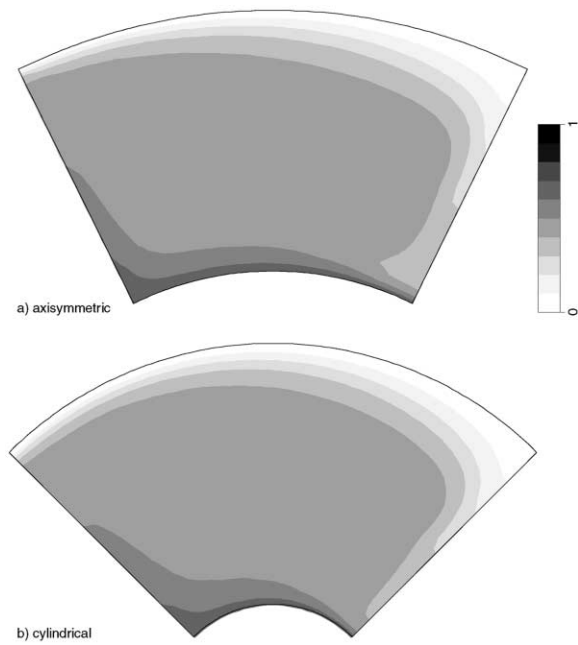


Fig. 5. Comparison of temperature in steady state bottom-heated convection in axisymmetric (a) and cylindrical geometry (b); $Ra = 10^6$, temperature-dependent rheology.

Table 4
Comparison for internally heated convection

| Geometry | Ra | q_t | v_{rms} | v_{max} | $\langle v \rangle$ | $\langle T_{bot} \rangle^a$ |
|-------------|-----------------|-------|-----------|-----------|---------------------|-----------------------------|
| Cylindrical | 5×10^4 | 6.38 | 26.7 | 58.0 | 31.5 | 1.60 |
| | 10^5 | 6.38 | 34.8 | 79.6 | 29.9 | 1.46 |
| | 2×10^5 | 6.39 | 48.1 | 117.2 | 39.9 | 1.32 |
| Spherical | 5×10^4 | 6.45 | 28.2 | 54.8 | 29.9 | 1.55 |
| | 10^5 | 6.46 | 36.7 | 75.3 | 37.7 | 1.42 |
| | 2×10^5 | 6.46 | 50.2 | 110.5 | 49.1 | 1.29 |

^a Average bottom temperature.

Table 5
Comparison of convection calculations with temperature-dependent viscosity

| Geometry | Ra | q_t | q_b | v_{rms} | v_{max} | $\langle v \rangle$ | $\langle \Phi \rangle$ |
|-------------|-----------------|-------|-------|-----------|-----------|---------------------|------------------------|
| Cylindrical | 5×10^5 | 2.608 | 8.71 | 91.6 | 59.2 | 39.8 | 0.91 |
| | 10^6 | 3.39 | 11.18 | 143.2 | 111.07 | 77.92 | 1.36 |
| | 2×10^6 | 4.61 | 14.77 | 229 | 219.5 | 157.6 | 2.46 |
| Spherical | 5×10^5 | 2.605 | 8.69 | 97.7 | 52.3 | 35.5 | 0.97 |
| | 10^6 | 3.27 | 10.84 | 148.3 | 92.08 | 65.0 | 1.34 |
| | 2×10^6 | 4.46 | 14.27 | 232 | 187.7 | 134.4 | 2.41 |

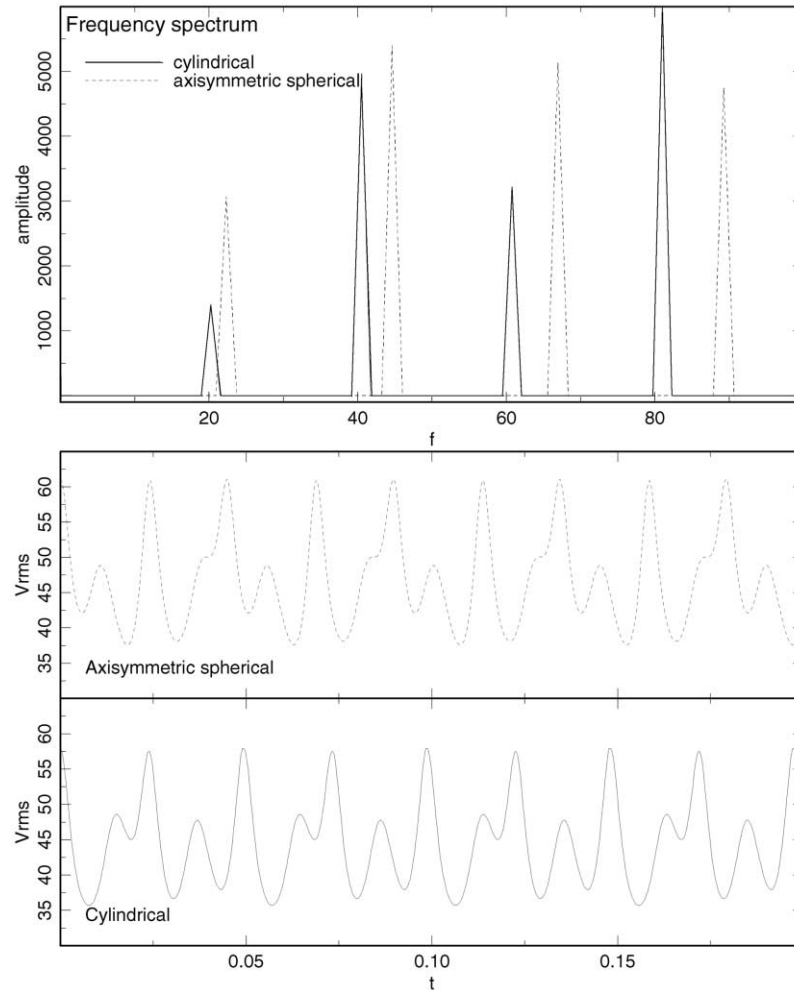


Fig. 6. Time-dependent comparison for internally heated model with rigid top and bottom boundary conditions. Both geometries display a P4 behavior. V_{rms} amplitude minima and maxima differ by only 5%. The difference in frequency is somewhat larger. Note that the convective vigor is rather moderate. In this scaling, the non-dimensional time $t = 1$ corresponds to 248 billion years.

internally heated benchmark of Blankenbach et al. (1989), where rigid boundary conditions are imposed at the top and bottom curves (Fig. 6). This benchmark uses the more restricted Boussinesq approximation, with $Di = 0$ and constant thermal diffusivity and expansivity. At low Ra , the flow is in steady state, but with increasing convective vigor the convection undergoes period doubling. As in the Cartesian benchmark, we use $Ra = 216,000$. In the Cartesian models, the behavior was found to be P2 (dominated by two periods), but this Ra is sufficiently close to a bifur-

cation that some participants in the 1989 benchmark found P4 behavior. The results obtained in axisymmetric spherical and (scaled) cylindrical geometry are plotted in Fig. 7. The power spectrum of the v_{rms} series shows a clear P4 behavior. Note that the flow obtained in the two geometries predict very similar behavior regarding periodicity and amplitude of the rms velocity, although the cylindrical model predicts slightly lower frequencies.

It is interesting to compare these results to those obtained in a cylindrical model without any scaling. To

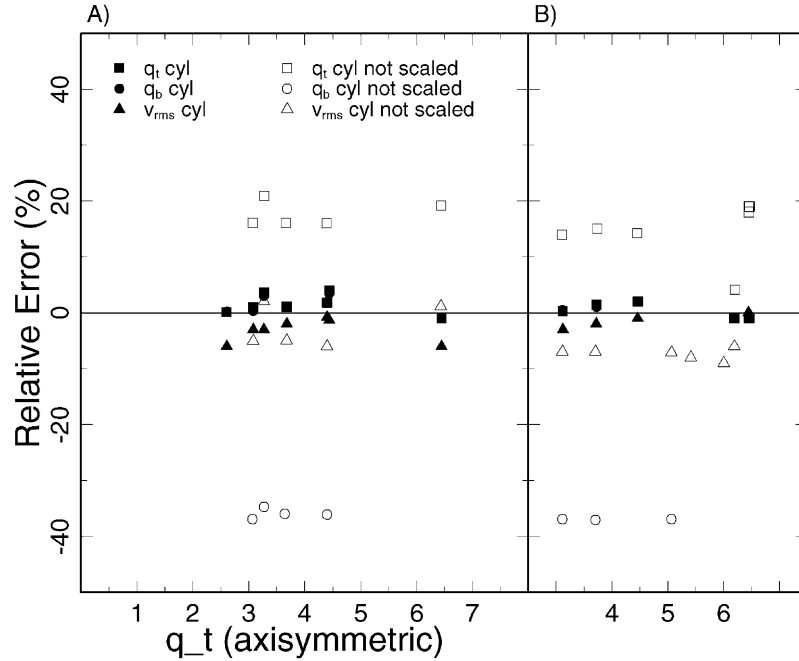


Fig. 7. Comparison of the error in derived quantities between cylindrical and axisymmetric spherical geometry for the scaled cylindrical geometry used in this study (solid symbols) and a cylindrical geometry without scaling (open symbols). The q_t represents surface heat flow, q_b bottom (or core) heat flow, and v_{rms} the root-mean-square velocity. The large errors caused by lack of curvature in the unscaled cylindrical models are significantly reduced by rescaling the radii of mantle and core. (A) Results based on those displayed in Figs. 3–5 and Tables 3–5. (B) Results based on complete extended Boussinesq approximation that includes the retention of variable ρ in the right-hand side of the Stokes Eq. (1) and pressure-dependent volumetric heating rate $Q = \rho H$, where H is the (constant) heating rate per mass unit.

this end, we recalculated the cylindrical steady state cases above using the unscaled non-dimensional radii $R_1 = 1.2083$ and $R_2 = 2.2083$ (see Fig. 2b). In general, the rms velocity is similar to that of the scaled cylindrical model, but the calculated heat flow values differ by up to 40%. We have summarized the results in Fig. 7a, where the relative error in derived quantities (defined as the relative difference with the result of the axisymmetric spherical calculation) are plotted as function of the surface heat flow in the axisymmetric spherical case. This provides an illustration of how strongly the results depend on convective vigor. Note that the error in derived quantities based on the scaled cylindrical models are less than a few percent, but that the heat flow errors for the unscaled cylindrical models are very large. There are no clear trends with increasing convective vigor noticeable.

We have made a similar set of comparisons as those shown in Figs. 3 and 4, but now taking into account

the depth dependence of ρ in the buoyancy term of Eq. (1) and the variable volumetric heat production. In effect, we use now $Q = \rho H$, where H is the (constant) heat production per unit mass. The difference between results of the two cylindrical approaches with those of the axisymmetric geometry are displayed in Fig. 7b, which compares well with the results shown in Fig. 7a.

To illustrate the impact of the scaling on secular cooling models, we compare the rescaled geometry with both parameterized convection and the unmodified cylindrical geometry (Fig. 8). The parameterized convection result is based on the solution of the heat balance,

$$(\rho_m c_m V_m + \rho_c c_c V_c) \frac{dT}{dt} = -q_t S_m + Q V_m \quad (13)$$

where V_m is the volume of the mantle, V_c the volume of the core, $\rho_c = 11,000 \text{ kg/m}^3$ the core density, $c_c = 500 \text{ J/kg K}$ the specific heat of the core, T

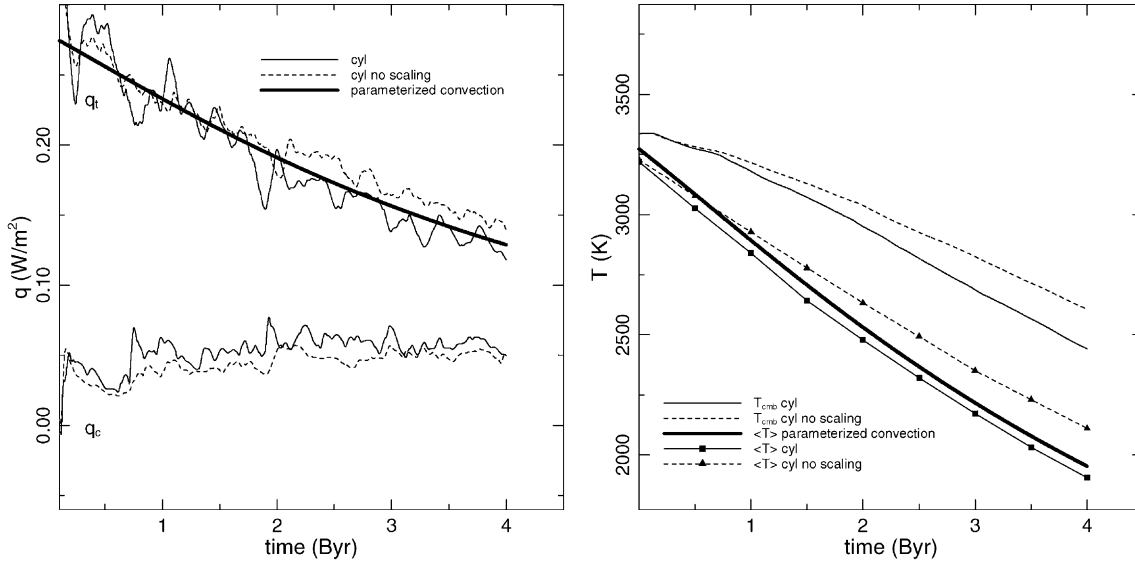


Fig. 8. Comparison of mantle evolution over 4 billion years using parameterized convection (bold lines), the scaled cylindrical approach (solid lines), and the non-scaled cylindrical approach (dashed lines). See text for full model description. The non-scaled cylindrical model overestimates the volume of the mantle, leading to too high internal heating, too high mantle temperature, and too high heat flow.

average mantle and core temperature, q_t the surface heat flow, S_m the surface area of the mantle, and Q the volumetric heating rate. The volumetric heating rate is based on the radiogenic heat production of U, Th, and K assuming bulk silicate Earth concentrations (e.g. Van Schmus, 1995). These values lead to a present day mantle heat production rate of 19.2 TW. The heat loss at the surface is described by assuming a standard power law dependence on Rayleigh number

$$q = 0.225Ra^{0.3} \quad (14)$$

(e.g. Turcotte and Schubert, 1982), where $Ra = \rho g \alpha \Delta T h^3 / \kappa \eta$. Here, we use the values shown in Table 2 and $\Delta T = T - T_s$, where $T_s = 273$ K is the surface temperature. This leads to a Rayleigh number close to 10^7 for $T = 3273$ K. The calculation is started 4 billion years ago, assuming an initial temperature of 3273 K. The heat balance equation is solved using a fourth-order Runge–Kutta scheme with a time step of 10 million years.

The fully dynamical simulations are calculated in a half cylinder (similar to that shown in Fig. 2a, but now for a 180° arc). The ‘scaled’ results are obtained using the mantle and core radii R_{2c} and R_{1c} , whereas

the ‘non-scaled’ results are obtained with the larger non-dimensional radii R_{2s} and R_{1s} (Fig. 2). The model description and solution methods are otherwise identical. Note that in this case, both simulations represent a cylindrical geometry. To better mimic the simplified physics of the parameterized convection calculation, we assume incompressible isoviscous flow with $Di = 0$ and constant thermodynamical properties. We start the simulation at 4 billion years ago using the same description for radiogenic heat production as in the parameterized convection simulation, assuming a constant temperature of $T = 3273$ K throughout the mantle, with the exception of a thin boundary layer at the top. During the simulation, the temperature of the core is updated using a simple cooling (or heating) expression based on the core heat flow,

$$\rho_c c_c V_c \frac{dT_c}{dt} = -q_c S_c \quad (15)$$

where S_c is the surface area of the core, T_c the core temperature, which is assumed to be identical to the temperature at the core–mantle boundary. Fig. 8 compares the results obtained using the three different approaches. Fig. 8a shows the mantle (q_t) and core

heat flow (q_c) for the scaled (solid) and non-scaled (dashed) cylindrical models, and the surface heat flow obtained from the parameterized convection calculation (bold). Fig. 8b shows the evolution of temperature in the models. The solid and dashed lines without symbols indicate the core–mantle boundary temperature for the scaled and non-scaled dynamical models. The bold line indicates the temperature predicted from the parameterized convection results, which represents the average mantle and core temperature. The average mantle and core temperature for the dynamical models are shown by the symbols. Due to radiogenic decay and secular cooling, the surface heat flow and mantle temperature steadily decrease. The scaled dynamical model is quite close in its evolution to that of the parameterized convection results. The non-scaled model overpredicts the volume of the lower mantle and as a consequence the overall radiogenic heat production is too high, which leads to an overestimate of average temperature (by about 200 K) and surface heat flow (by about 25 mW/m²).

4. Discussion and conclusions

The results presented above clearly illustrate that the use of a scaled cylindrical geometry is beneficial to enhance the curvature and make the cylindrical geometry more useful for comparison with a fully spherical model. For steady state results, obtained at moderate convective vigor, the derived quantities such as heat flow and rms velocity agree to within a few percent from the axisymmetric spherical results. This conclusion holds for bottom and internal heating, isoviscous and moderately temperature-dependent rheology, as well as steady state and time-dependent simulations. These conclusions are based on benchmarks at moderate convective vigor, but a summary of the error as function of surface heat flow (Fig. 7) indicates that there is no strong trend with increasing convective vigor. An explicit comparison with parameterized convection models at realistic Earth-like convective vigor shows that the scaling used in this paper provides a significantly better match than the non-scaled results which overpredicts the significance of radiogenic heating.

While studying this particular scaling, we encountered a number of other possibilities that appeared

to provide a satisfying scaling of heat production or surface heat loss. For example, imagine a cylindrical model with non-scaled mantle and core radii, with constant internal heating and no bottom heating. One could calculate the change in surface-to-volume ratio from the spherical case, and apply a correcting factor to the cylindrical model. However, this approach is in jeopardy as soon as bottom heating is introduced, as the surface of the core–mantle boundary is too large compared to the spherical geometry. Another complication occurs when depth-dependent heat production is assumed, as the surface-to-volume ratio is not a constant as function of depth. The correction would then require a depth-dependent correction term. These complications are avoided with the scaling used here.

Due to the very high cost still associated with 3D fully spherical models, we anticipate that geometrical simplifications (that reduce the geometry effectively to 2D) will remain popular for a significant amount of time. Due to the drawbacks associated with axisymmetric spherical geometry and (to a lesser extent) Cartesian geometry, we recommend the use of this scaled cylindrical geometry. This is of particular importance for those convection studies that attempt to model secular evolution of the Earth, as the scaled cylindrical models provide heat-transport properties that are much closer to those of the spherical Earth.

Acknowledgements

Discussions with Scott King, Geoff Davies, Henry Pollack, and Allen McNamara are greatly appreciated. Constructive reviews from Ulrich Christensen, the editor Ken Creager, and an anonymous reviewer are gratefully acknowledged.

References

- Bercovici, D., Schubert, G., Glatzmaier, G.A., 1989. Three-dimensional spherical models of convection in the Earth's mantle. *Science* 244, 950–955.
- Blankenbach, B., Busse, F., Christensen, U., Cserepes, L., Gunkel, D., Hansen, U., Harder, H., Jarvis, G., Koch, M., Marquart, G., Moore, D., Olson, P., Schmeling, H., Schnaubelt, T., 1989. A benchmark comparison for mantle convection codes. *Geophys. J. Int.* 98, 23–38.

- Bunge, H.P., Richards, M.A., Baumgardner, J.R., 1996. Effect of depth-dependent viscosity on the planform of mantle convection. *Nature* 379, 436–438.
- Busse, F.A., Christensen, U., Clever, R., Cserepes, L., Giannandrea, E., Guillou, L., Nataf, H.-C., Ogawa, M., Parmentier, M., Sotin, C., Travis, B., 1993. Convection at infinite Prandtl number in Cartesian geometry — a benchmark comparison. *Geophys. Astrophys. Fluid Dyn.* 75, 35–59.
- Christensen, U.R., 1985. Thermal evolution models of the Earth. *J. Geophys. Res.* 90, 2995–3007.
- Cuvelier, C., Segal, A., Van Steenhoven, A.A., 1986. *Finite Element Methods and the Navier–Stokes Equations*. Reidel, Dordrecht.
- Ita, J., King, S.D., 1994. Sensitivity of convection with an endothermic phase change to form of governing equations, initial conditions, boundary conditions and equation of state. *J. Geophys. Res.* 99, 15919–15938.
- Jarvis, G.T., 1994. The unifying role of aspect ratio in cylindrical models of mantle convection with varying degrees of curvature. *Geophys. J. Int.* 117, 419–426.
- Jarvis, G.T., McKenzie, D.P., 1980. Convection in a compressible fluid with infinite Prandtl number. *J. Fluid Mech.* 96, 515–583.
- Leitch, A.M., Yuen, D.A., Sewell, G., 1991. Mantle convection with internal heating and pressure-dependent thermal expansivity. *Earth Planet. Sci. Lett.* 102, 213–232.
- Machetel, P., Yuen, D.A., 1988. Infinite Prandtl number spherical shell convection. In: Vlaar, N.J., Nolet, G., Wortel, M.J.R., Cloetingh, S.A.P.L. (Eds.), *Mathematical Geophysics*. Reidel, Norwell, MA, pp. 265–290.
- McNamara, A.K., Van Keken, P.E., 2000. Cooling of the Earth: a Parameterized Convection Study of Whole vs. Layered Models, *G³*, Vol. 1.
- Pollack, H.N., Hurter, S.J., Johnston, R., 1993. Heat loss from the Earth's interior: analysis of the global data set. *Rev. Geophys.* 31, 267–280.
- Solheim, L.P., Peltier, W.R., 1994. Avalanche effects in phase transition modulated thermal convection — a model of Earth's mantle. *J. Geophys. Res.* 99, 6997–7018.
- Spohn, T., Schubert, G., 1982. Modes of mantle convection and the removal of heat from the Earth's interior. *J. Geophys. Res.* 87, 4682–4696.
- Tackley, P.J., 2000. Mantle convection and plate tectonics: toward an integrated physical and chemical theory. *Science* 288, 2002–2007.
- Tackley, P.J., Stevenson, D.J., Glatzmaier, G.A., Schubert, G., 1993. Effects of an endothermic phase transition at 670 km depth in a spherical model of convection in the Earth's mantle. *Nature* 361, 699–704.
- Turcotte, D.L., Schubert, G., 1982. *Geodynamics, Applications of Continuum Physics to Geological Problems*. Wiley, New York, 450 pp.
- Van den Berg, A.P., Van Keken, P.E., Yuen, D.A., 1993. The effects of a composite non-Newtonian and Newtonian rheology on mantle convection. *Geophys. J. Int.* 115, 62–78.
- Van Keken, P.E., Ballentine, C.J., 1999. Dynamical models of mantle volatile evolution and the role of phase changes and temperature-dependent rheology. *J. Geophys. Res.* 104, 7137–7169.
- Van Keken, P.E., Yuen, D.A., 1995. Dynamical influences of high viscosity in the lower mantle induced by the steep melting curve of perovskite: effects of curvature and time dependence. *J. Geophys. Res.* 100, 15233–15248.
- Van Keken, P.E., King, S.D., Schmeling, H., Christensen, U.R., Neumeister, D., Doin, M.P., 1997. A comparison of methods for the modeling of thermochemical convection. *J. Geophys. Res.* 102, 22477–22495.
- Van Schmus, W.R., 1995. Natural radioactivity of the crust and mantle. In: Ahrens, T.J. (Ed.), *Global Earth Physics, A Handbook of Physical Constants*, AGU Reference Shelf 1. American Geophysical Union, Washington, DC, pp. 283–291.
- Vangelov, V.I., Jarvis, G.T., 1994. Geometrical effects of curvature in axisymmetrical spherical models of mantle convection. *J. Geophys. Res.* 99, 9345–9358.
- Zhang, S.X., Yuen, D.A., 1996. Various influences on plumes and dynamics in time-dependent, compressible mantle convection in 3D spherical shell. *Phys. Earth Planet. Int.* 94, 241–267.